Journal of Biomechanics 52 (2017) 113–121

Contents lists available at ScienceDirect

Journal of Biomechanics

journal homepage: www.elsevier.com/locate/jbiomech
www.JBiomech.com

Instantaneous centers of rotation for lumbar segmental extension in vivo

Ameet Aiyangar [a], Liying Zheng [d,e], William Anderst [b], Xudong Zhang [b,c,d,*]

[a] Empa, Swiss Federal Laboratories for Materials Science and Technology, Mechanical Systems Engineering, Ueberlandstrasse 129, 8600 Duebendorf, Switzerland
[b] Department of Orthopaedic Surgery, University of Pittsburgh, Pittsburgh, PA 15203, USA
[c] Department of Bioengineering, University of Pittsburgh, Pittsburgh, PA 15203, USA
[d] Department of Mechanical Engineering and Materials Science, University of Pittsburgh, Pittsburgh, PA 15203, USA
[e] Health Effects Lab Division, National Institute for Occupational Safety and Health, Morgantown, West Virginia, 26505, USA

ARTICLE INFO

Article history:
Accepted 19 December 2016

Keywords:
Lumbar spine
Vertebral motion
Instantaneous center of rotation
Dynamic stereo X-ray
Lifting task

ABSTRACT

The study aimed to map instantaneous centers of rotation (ICRs) of lumbar motion segments during a functional lifting task and examine differences across segments and variations caused by magnitude of weight lifted. Eleven healthy participants lifted loads of three different magnitudes (4.5, 9, and 13.5 kg) from a trunk-flexed (~75°) to an upright position, while being imaged by a dynamic stereo X-ray (DSX) system. Tracked lumbar vertebral (L2-S1) motion data were processed into highly accurate 6DOF inter-vertebral (L2L3, L3L4, L4L5, L5S1) kinematics. ICRs were computed using the finite helical axis method. Effects of segment level and load magnitude on the anterior-posterior (AP) and superior-inferior (SI) ICR migration ranges were assessed with a mixed-effects model. Further, ICRs were averaged to a single center of rotation (COR) to assess segment-specific differences in COR AP- and SI-coordinates. The AP range was found to be significantly larger for L2L3 compared to L3L4 ($p=0.02$), L4L5 and L5S1 ($p<0.001$). Average ICR SI location was relatively higher – near the superior endplate of the inferior vertebra – for L4L5 and L5SI compared to L2L3 and L3L4 ($p\leq 0.001$) – located between the mid-transverse plane and superior endplate of the inferior vertebra – but differences were not significant amongst themselves ($p>0.9$). Load magnitude had a significant effect only on the SI component of ICR migration range (13.5 kg > 9 kg and 4.5 kg; $p=0.049$ and 0.017 respectively). The reported segment-specific ICR data exemplify improved input parameters for lumbar spine biomechanical models and design of disc replacements, and base-line references for potential diagnostic applications.

1. Introduction

Lumbar spinal motion has predominantly been characterized in terms of relatively simple metrics, such as end-range of rotational motion (ROM) occurring about a fixed, average center of rotation (COR) (Cossette et al., 1971; Freudiger et al., 1999; Fujii et al., 2007; Ochia et al., 2006; Pearcy et al., 1984; White and Panjabi, 1978; Xia et al., 2010). However, lumbar motion comprises rotational and translational components (Aiyangar et al., 2014; Gertzbein et al., 1984; Ogston et al., 1986; Xia et al., 2010), and motion at different intervals may exhibit different characteristics, particularly between healthy and pathologically or surgically altered spines (Ahmadi et al., 2009; Ellingson and Nuckley, 2015; Natarajan et al., 2008; Passias et al., 2011). Hence, comprehensive characterization of vertebral kinematics should ideally incorporate the spatial and temporal variations of both rotational and translational components. Within this context, mapping the locus of *instantaneous* centers of rotation (ICRs) between two adjacent vertebrae over a given motion – the centrode – has been shown to be a reasonable way to simultaneously quantify the translational component of lumbar motion and its coupling with the rotational component. More importantly, the ICR has been shown to have a biological basis linking aberrations in its location to anatomical and pathological factors, based on its strong association with the center of reaction (Bogduk et al., 1995; Schneider et al., 2005; Zander et al., 2016). *In vitro* as well as some *in vivo* studies have shown promising results in applying spatial variations in ICR paths to distinguish between healthy lumbar spines and those with segmental instability (Ahmadi et al., 2009; Gertzbein et al., 1986) as well as different degrees of disc degeneration (Ellingson and Nuckley, 2015; Gertzbein et al., 1985). Modelling studies have demonstrated how even small variations in implant placement and design could

* Corresponding author at: Department of Industrial & Systems Engineering, Texas A&M University, College Station, TX 77843-3131, USA. Fax: +1 979 458 4299.
E-mail address: xuz9@pitt.edu (X. Zhang).

http://dx.doi.org/10.1016/j.jbiomech.2016.12.021
0021-9290/

elicit notable alterations in load distribution patterns on the facets and adjacent segments (Han et al., 2013; Zander et al., 2009). Furthermore, accurate task-specific ICR information is a crucial input for inverse kinematics-driven biomechanical models, as the estimation of muscle moment arms and, consequently, muscle and joint forces can be highly sensitive to small changes in the presumed location of the COR (Abouhossein et al., 2013; Han et al., 2013; Zhu et al., 2013) and, by association, the center of reaction (Bogduk et al., 1995; Schneider et al., 2005; Zander et al., 2016).

Although ICRs and centrode patterns have been estimated using the *method of Reuleaux* from a series of static radiographs (Gertzbein et al., 1984, 1985, 1986; Ogston et al., 1986), the lack of sufficient precision has hampered the confidence level in past reported data (Crisco et al., 1994; Pearcy et al., 1984). Developments in dynamic radiographic imaging techniques over the last decade, however, have overcome these limitations to afford more accurate measurement of *in vivo* vertebral motion during functional activities (Ahmadi et al., 2009; Aiyangar et al., 2015, 2014; Anderst et al., 2008; Teyhen et al., 2007; Wong et al., 2004; Wu et al., 2014).

Our systematic endeavor to map three-dimensional (3D) kinematics of the healthy lumbar spine has been motivated by these developments. The current study investigates lumbar ICR migration patterns during a functional lifting task and poses the following hypotheses:

(1) ICR migration patterns vary across the individual lumbar segments, both in the anterior-posterior (AP) and superior-inferior (SI) directions. Specifically,
   a. The range of ICR migration varies across the lumbar segments.
   b. The locations of the ICRs, as defined relative to the inferior vertebra of a given intervertebral segment, vary across the segments.
(2) The magnitude of load lifted has a significant effect on the location and the migration range of the ICRs.

2. Materials and methods

With Institutional Review Board approval, 14 healthy participants (eight male, six female) between the ages of 19 and 30 years (24 ± 2) and a waist size no greater than 89 cm (35 in) [$x(S) = 79 \pm 8$ cm (31 ± 3 in)] were recruited for the study. Mean height and weight of participants were 175 (± 8) cm and 71 (± 12) kg respectively. Participants reported no prior history of lower back disorders. All participants provided written, informed consent.

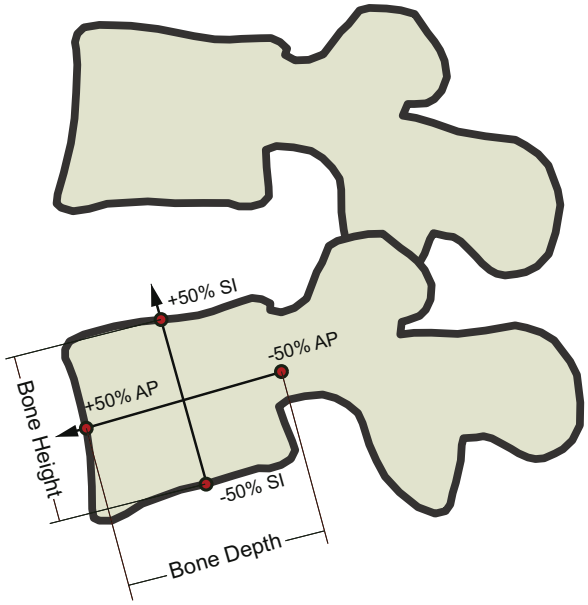

Fig. 1. Normalizing absolute ICR coordinates in terms of vertebral body height and depth. 100% represents total height (mid-coronal plane) and depth (mid-sagittal plane) of the inferior vertebra of each intervertebral segment in the SI- and AP directions respectively, with the origin located at the center of the vertebral body. Superior and inferior endplates have an ordinate value of +50% and −50% respectively. Similarly, abscissa values for most anterior point and most posterior point are +50% and −50% respectively.

Starting from a trunk-flexed (~75° flexion) position, participants lifted a known load anteriorly and close to the body [three load weights: 4.54 kg (10 lb), 9.1 kg (20 lb) and 13.6 kg (30 lb)] up to an upright position in a sagittally symmetric manner primarily with trunk extension without knee bending. Pelvic motion was partially limited by having participants maintain a light but constant contact with a semi-rigid *pelvic rest* placed behind them so as to remain within the field of view of the medial-lateral camera system, but otherwise unconstrained (Aiyangar et al., 2014). Participants performed a maximum of six trials (two per load level), each taking two seconds or less.

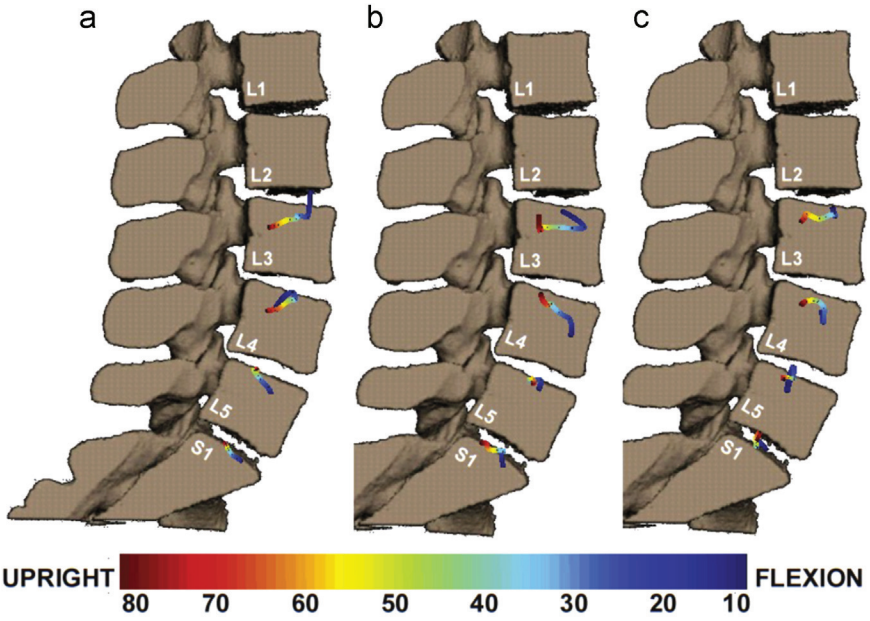

Fig. 2. Instantaneous centers of rotation (ICR) for each intervertebral segment superimposed onto a representative lumbar spine bone model for the three weight lifting tasks: (a) 4.54 kg (10 lb), (b) 9.1 kg (20 lb) and (c) 13.6 kg (30 lb). Color map indicates progression of extension motion (flexion to upright) from 10% to 80% of L2-S1 ROM. Black dots represent the ICRs averaged across all participants at every decile (10%, 20% …80%) of overall L2-S1 extension. (For interpretation of the references to color in this figure legend, the reader is referred to the web version of this article.)

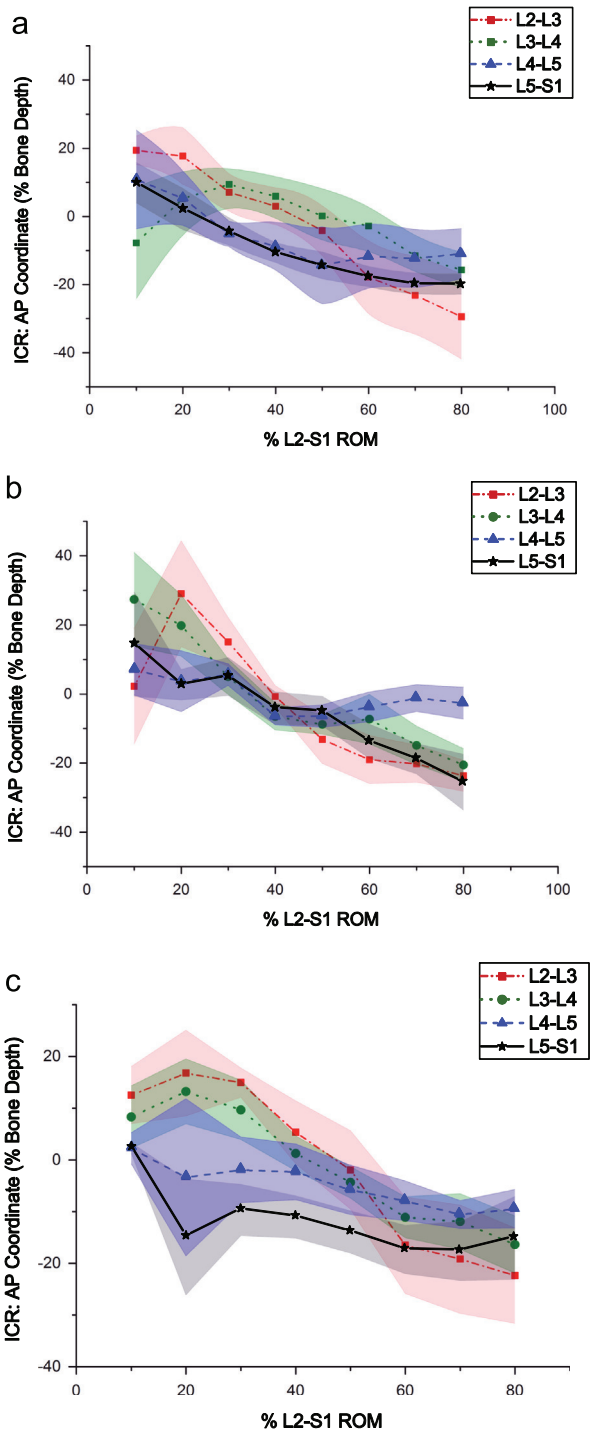

Fig. 3. Time series plots of showing anterior-posterior (AP) component of ICR migration for each lumbar segment with respect to progression of extension motion, expressed as %L2-S1 ROM, for the three weight lifting tasks: (a) 4.54 kg (10 lb), (b) 9.1 kg (20 lb) and (c) 13.6 kg (30 lb). % L2-S1 ROM is a surrogate for "time". Error bars indicate 95% confidence interval of the mean, AP ICR coordinate at every decile of %L2-S1 ROM normalized to corresponding inferior vertebral body depth.

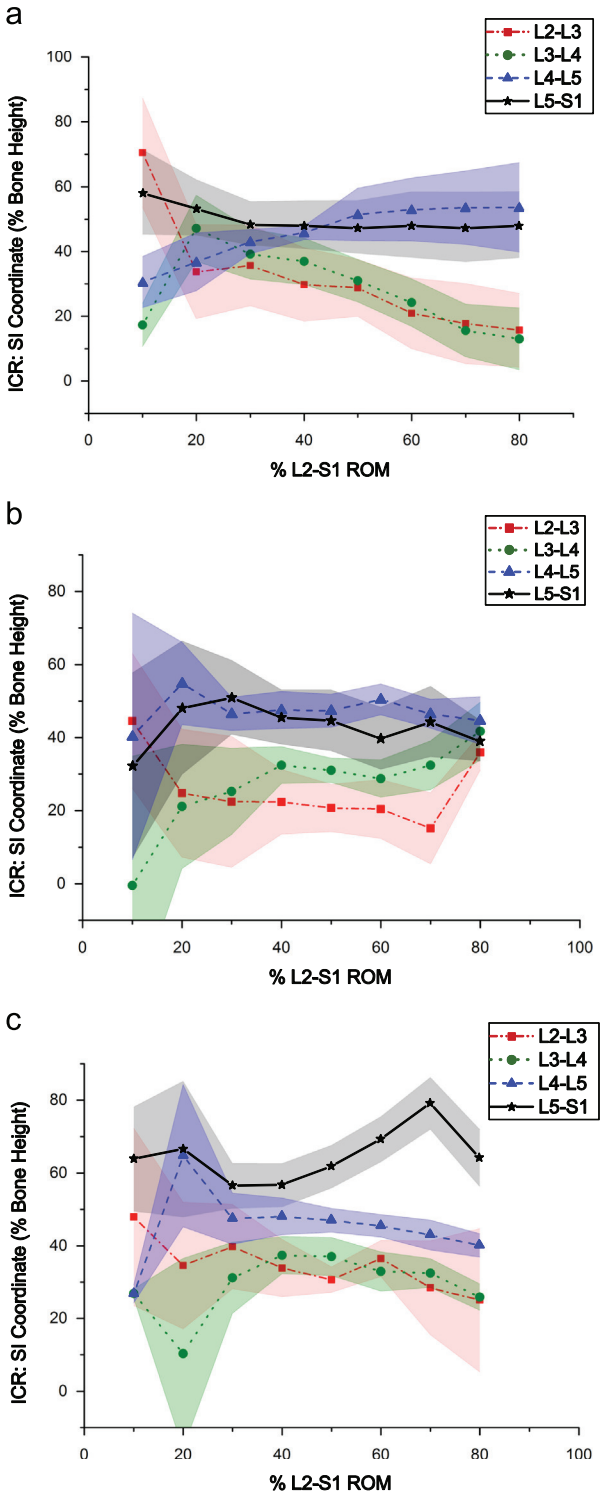

Fig. 4. Time series plots of showing superior-inferior (SI) component of ICR migration for each lumbar segment with respect to progression of extension motion, expressed as %L2-S1 ROM, for the three weight lifting tasks: (a) 4.54 kg (10 lb), (b) 9.1 kg (20 lb) and (c) 13.6 kg (30 lb). % L2-S1 ROM is a surrogate for "time". Error bars indicate 95% confidence interval of the mean SI ICR coordinate at every decile of %L2-S1 ROM, normalized to corresponding inferior vertebral body height (L5S1 data are normalized to height of L5).

Participants' lumbar regions (L2-S1) were imaged using a dynamic stereo X-ray (DSX) system in ML- and AP directions (60 *frames at* 30 fps, *pulsed exposure time*=4 ms/frame, *excitation voltage*=70–80 kV, *current*=320–630 mA). The AP camera and intensifier were angled at $\pm 30^{\circ}$ respectively, with regard to the horizontal plane to obviate excessive attenuation of X rays by the upper body. X-ray images recorded with high-speed cameras (4 megapixel Phantom v10, Vision Research) from 16-in. image intensifiers were mapped to images of dimensions 1800×1824 pixels (pixel size ~ 0.22 mm) and down-sampled to 512×512 pixel resolution ($\sim 0.8 \times 0.8$ mm^2 pixel size), which was previously shown to increase tracking speed without a noticeable reduction in accuracy (Martin et al., 2011).

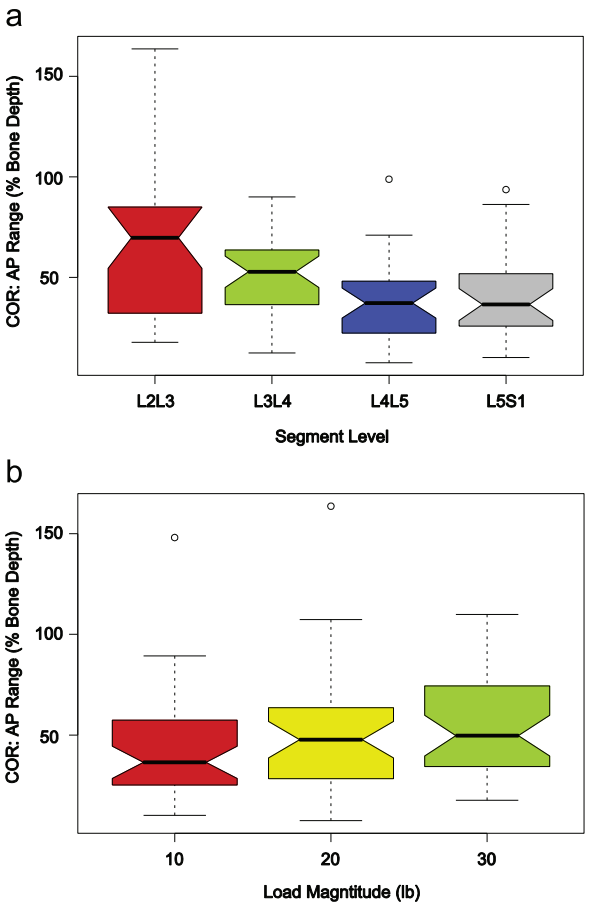

Fig. 5. AP component of the range of ICR migrations across (a) the observed intervertebral segments L23, L34, L45 and L5S1, and (b) the three weight lifting tasks: 4.54 kg (10 lb), 9.1 kg (20 lb) and 13.6 kg (30 lb). 5a presents the main effect of segmental level and includes results from all three weight lifting tasks. 5b presents the main effect of load magnitude and includes results from all the four intervertebral segments. Magnitudes are normalized to the corresponding inferior vertebral body depth. 100% represents the whole depth of the vertebral body. Lack of overlap in notches of box plots qualitatively indicates significant differences.

Table 1
Segmental level- and load magnitude-specific magnitudes of the loci of ICR (centrode).

Extension ROM °($\pm$ CI_{95})	Lumbar segment	Centrode ($\pm$ 95% CI) (% vertebral body depth)			
		10lb	20lb	30lb	All tasks
9.9 (1.5)	L2-L3	124 (32)	117 (35)	128 (49)	122 (21)
10.7 (1.4)	L3-L4	109 (28)	100 (25)	103 (21)	104 (14)
12.1 (2)	L4-L5	86 (24)	110 (30)	109 (24)	103 (15)
9.6 (2.1)	L5-S1	124 (42)	124 (45)	146 (46)	130 (25)

High resolution computed tomography (CT) scans *(voxel size* = 0.25 mm × 0.25 mm × 1.25 mm; *GE Lightspeed Pro 16, GE Medical Systems, Waukesha, WI)* of participants' lumbar spines were also obtained. Individual vertebrae were segmented to create 3D bone models using Mimics 14.0 *(Materialise Inc., Ann Arbor, MI)*. Estimated total effective radiation dose from DSX for all lifting trials combined, determined using PCXMC simulation software *(STUK, Helsinki, Finland)*, was less than 3.6 mSv, while maximum estimated effective CT radiation dose was less than 12.33 mSv.

A previously validated model-based tracking process was used to determine instantaneous 3D vertebral positions for all static and dynamic trials with sub-millimeter accuracy {precision $\leq$ 0.26°, 0.2 mm (Lee, 2010)}. Detailed descriptions of the procedure can be found here (Aiyangar et al., 2014; Anderst et al., 2008; Lee, 2010).

Vertebral anatomical coordinate systems (ACS) (Wu et al., 2002) were defined by three mutually orthogonal axes – AP, ML, and superior-inferior (SI) – with the origin at the vertebral body center. Ordered body-fixed rotations and translations

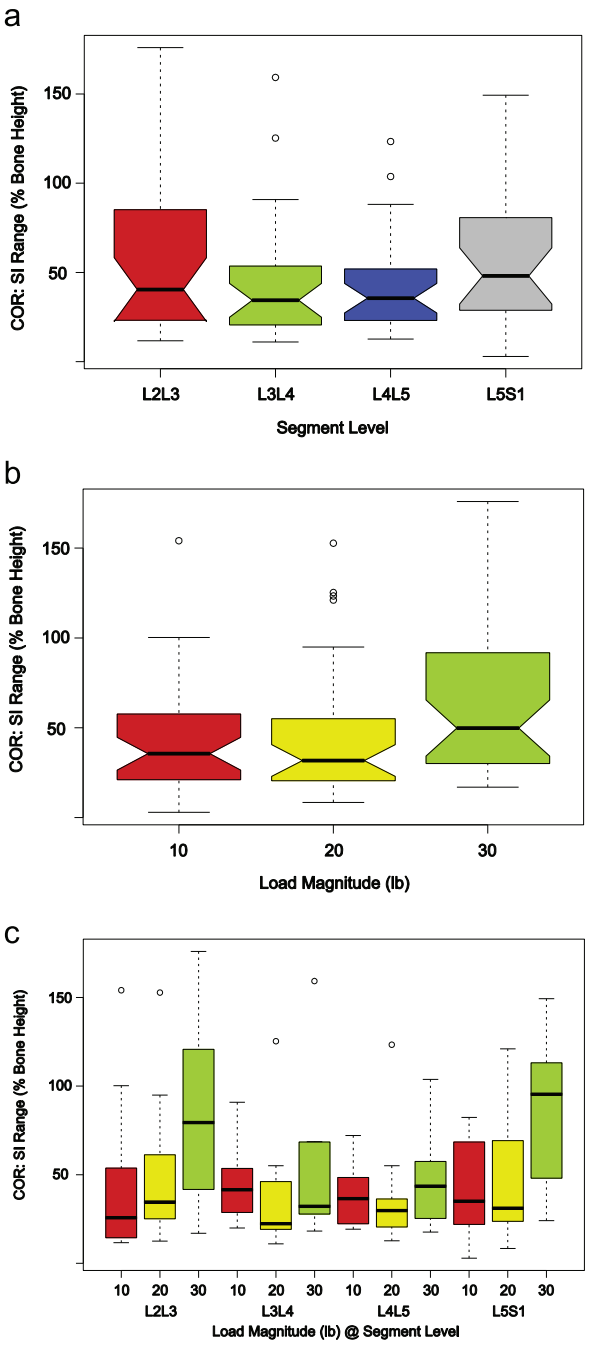

Fig. 6. SI component of the range of ICR migrations: (a) across the observed intervertebral segments L23, L34, L45 and L5S1, (b) across the three weight lifting tasks: 4.54 kg (10 lb), 9.1 kg (20 lb) and 13.6 kg (30 lb) and (c) for each segment divided by each weight lifting task: e.g.: 10.L23 represents the value for L23 segment for the 4.5 kg (10 lb) lifting trial. 6a presents the main effect of segmental level and includes results from all three weight lifting tasks. 6b presents the main effect of load magnitude and includes results from all the four intervertebral segments. Magnitudes are normalized to the corresponding inferior vertebral body height (L5S1 data are normalized to height of L5). 100% represents the whole height of the vertebral body. Lack of overlap in notches of box plots qualitatively indicates significant differences.

were extracted to express segmental (L2L3, L3L4, L4L5, and L5S1) motion by relating frame-by-frame position of the superior vertebral ACS relative to the inferior vertebral ACS.

The following steps were applied to normalize the kinematics to allow their representation simultaneously across all segments, trials and participants. First, segmental kinematics were initialized to the starting flexed position. Next, in order to standardize the abscissa across all trials and participants, the starting flexed overall L2-S1 pose assumed for the lifting task was defined as 0%, with the pose in the final

Table 2
Segmental level- and load magnitude-specific migration ranges in AP and SI directions (dissimilar superscripts indicate significant difference).

Lumbar segment	A-P range (± 95% CI) (% vertebral body depth)				S-I range (± 95% CI) (% vertebral body height)			
	10lb	20lb	30lb	All tasks	10lb	20lb	30lb	All tasks
L2-L3	62 (19)	71 (19)	64 (18)	**65 (14)**[a]	45 (24)	56 (26)	64(25)	**54 (16)**
L3-L4	44 (14)	48 (10)	57 (15)	**52 (9)**[ab]	43 (14)	41 (19)	45 (20)	**40 (10)**
L4-L5	34 (12)	36 (10)	47 (15)	**38 (8)**[b]	37 (12)	36 (15)	47 (15)	**42 (10)**
L5-S1	48 (20)	47 (20)	49 (13)	**41 (10)**[b]	47 (16)	51 (25)	74 (27)	**57 (16)**

recorded frame presumed as 100% (100_{temp}). Now, the L2-S1 pose at the end of the lifting task may not have matched each participant's static upright L2-S1 pose. Hence, each participant's static upright posture was assigned as the new end reference point representing 100% (100_{final}). L2-S1 extension, expressed as a percentage of total completed ROM, was then corrected by multiplying a weighting factor ($100_{temp}/100_{final}$) representing the fraction of the "ideal" achievable amount of L2-S1 extension – static upright pose – reached by the participant in that particular trial. (*Note: The correction factor was not applied to individual segmental kinematics, rather only to the %L2-S1 ROM for purposes of defining the abscissa.*) This scaling allowed 100% of L2-S1 extension motion to be defined universally for each trial as the individual participant's static upright posture rather than the pose from the last recorded frame and standardized the *abscissa* for all participants (0–100% of L2-S1 ROM).

Instantaneous segmental axes of rotation were computed using the finite helical axis (FHA) method at 0.5° segmental extension increments (Baillargeon and Anderst, 2013). ICRs were defined as piercing points of the FHA through the mid-sagittal plane according to $n^T n = 1; n^T s = 0$ (Spoor and Veldpaus, 1980), where: $\boldsymbol{n}$=*helical axis, located in the axial plane;* $\boldsymbol{s}$=*orthogonal vector from ACS origin, located in the mid-sagittal plane*. The following additional normalization steps enabled simultaneous visualization and comparison of segmental ICRs across all participants, segments and load lifting tasks (Fig. 1): Centrodes were computed by summing distances between each successive ICR for a given trial and normalized to vertebral depth. ICR ranges were then computed separately in AP and SI directions and normalized to corresponding depth and height respectively. Segmental ICRs were interpolated to obtain ICRs at every decile (10%, 20%… 80%) of total L2-S1 ROM. Finally, AP- and SI-coordinates of interpolated ICRs were also normalized to vertebral depth and height respectively.

2.1. Statistical analysis

Where data were successfully recorded from both trials per load for any given participant, the two datasets were averaged into a single dataset to represent the participant's motion for subsequent analysis. Mean ($\pm CI_{95}$) segmental ICR AP- and SI-coordinates for every decile of L2-S1 extension ROM were computed for each load-lifting task across participants to enable qualitative observations of differences across segments and across load levels. Time series plots ("time", as indicated by % L2-S1 ROM progression) of the AP- and SI- ICR coordinates between 10% and 80% of L2-S1 ROM were generated and corresponding linear regression-based slopes were computed to identify migration trends, demonstrated by a slope significantly different from zero (α=0.05).

In order to evaluate segmental level- and loading-specific differences in ICR location, the instantaneous AP- and SI-coordinates were aggregated (collapsed over time) to provide mean load magnitude- and segment-specific centers of rotation (CORs). Repeated Measures Analysis (Anderst et al., 2013; Kozanek et al., 2009; Li et al., 2011; Xia et al., 2010) was employed with data compiled as a mixed model, with segmental level (four levels: L2L3, L3L4, L4L5, L5S1) and load magnitude (three levels: 4.54 kg, 9.1 kg, 13.6 kg) as the two within-subject, fixed effect, categorical factors and "participant" as the random factor. Mean SI COR coordinate, AP- and SI-ranges of ICR migration were the outcome variables. Differences between segments and load magnitudes were assessed based on post-hoc Tukey Honest Significant Difference (HSD) comparison-of-means tests. The extent of overlap between the $\pm CI_{95}$ values, and also between notches of the respective boxes in the notched box plots (Mcgill et al., 1978; R_Core_Team, 2015), provided a visual albeit qualitative representation of the differences between the groups. The notches extend to [± 1.58*IQR/((n) $^{0.5}$)], where "IQR"=interquartile range between first to third quartile, and "n"=number of non-missing observations within the group. In both cases, no overlap indicated significant differences. All calculations were performed in R® Statistical Software (R_Core_Team, 2015).

3. Results

Of the 14 participants, data from three were omitted due to poor image quality. Six out of the 122 segmental ICR datasets (4.9%) processed were deemed outliers and excluded, as their AP or SI range of ICR migration exceeded 175% ($\sim 3\times$ mean value), or their centrodes exceeded 250% of bone depth ($\sim 2\times$ mean value) (Baillargeon and Anderst, 2013), or both.

Substantial migration of ICRs was observed at all segments (Fig. 2, Table 1). Barring a few exceptions, ICRs generally migrated from anterior to posterior as motion progressed (Figs. 3 and 4). Statistically significant negative slopes (from anterior to posterior) from the linear fit for AP component of ICR migration were found for every segment at each load case ($p < 0.05$). In contrast, a majority of slopes for SI ICR migration did not reveal evidence of a trend.

Including segment-load magnitude interaction in the repeated measures model resulted in none of the factors exerting statistically significant effects on either the COR or AP- and SI-components of the range of ICR migration. The interaction factor was highly correlated with load magnitude and segment level – an indication of either multi-collinearity or inadequate sample size – hence was dropped from the model. The main effect of segment level on AP range of ICR migration was significant: Tukey HSD tests revealed significantly larger AP migration of ICRs in the L2L3 segment compared to other segments. (L3L4: p=0.02; L4L5 and L5S1: $p < 0.001$). No significant differences were detected between the other segments (L3L4/L4L5: p=0.06; L3L4/L5S1: p=0.32; L4L5/L5S1: p=0.9). Notched box plots provide a visual representation of these segment-wise differences (Fig. 5a). Although there appeared to be a mild effect of load magnitude (p=0.048, Fig. 5b), post-hoc comparisons did not reveal significant effects between the three loads lifted ($p > 0.1$), implying a minimal effect, if any, on overall model fit.

Segment level did not appear to have a significant effect on SI range of ICR migration ($p > 0.6$), but a moderate yet significant effect of load magnitude was detected (Fig. 6): lifting the heaviest load (13.6 kg) resulted in a larger SI component of ICR migration compared to the two lighter loads (9.1 kg: p=0.049; 4.54 kg: p=0.017). Mean ($\pm CI_{95}$) values for AP- and SI- migration ranges are presented in Table 2.

Averaged COR SI coordinates were located approximately midway between the mid-transverse plane and superior endplate of inferior vertebra for the cranial segments, L2L3 *[median* ($\pm$ IQR)=34 $\pm$ 6%] and L3L4 [median ($\pm$ IQR)=33 $\pm$ 5%]. Comparatively, averaged COR SI coordinates for L4L5 and L5S1 were located substantially higher, closer to the superior endplate of their respective inferior vertebrae [median ($\pm$ IQR)=43 $\pm$ 4% and 52 $\pm$ 5% respectively] (Fig. 7a, Table 3). Segment level had a significant effect: the cranial segments were significantly different from the caudal segments (L5S1 and L4L5 vs. L2L3: $p < 0.001$; L5S1 vs. L3L4: p=0.0011; L4L5 vs. L3L4: p=0.004; L5S1 vs. L4L5: p=0.98 and L2L3 vs. L3L4: p=0.91) and depicted graphically by the notched boxplots (Fig. 7a). Significant effect of load magnitude was not detected (p=0.62); Fig. 7b). AP COR coordinates converged onto – or slightly posterior to – the mid-coronal plane of the inferior vertebral body (Table 3). Neither load magnitude nor segment level effected significant differences on the averaged AP COR coordinates.

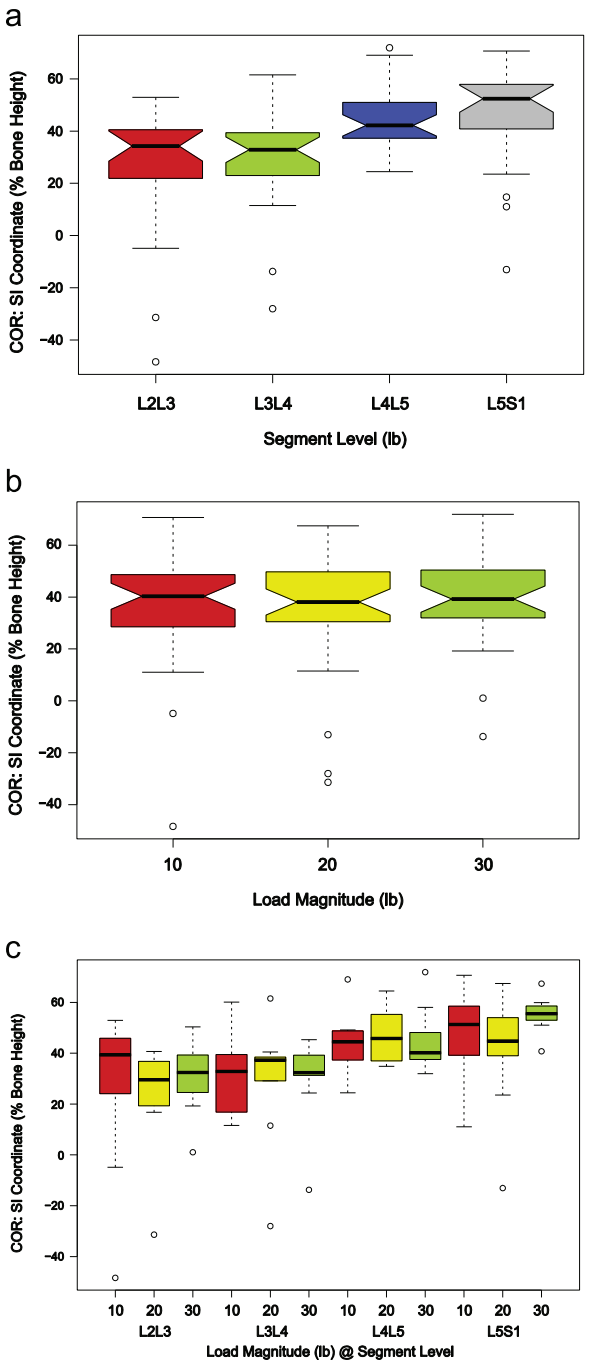

Fig. 7. SI coordinates of the Center of rotation (COR): (a) across the observed intervertebral segments L23, L34, L45 and L5S1; (b) across the three weight lifting tasks: 4.54 kg (10 lb), 9.1 kg (20 lb) and 13.6 kg (30 lb) and (c) for each segment divided by each weight lifting task: e.g.: 10.L23 represents the value for L23 segment for the 4.5 kg (10 lb) lifting trial. 7a presents the main effect of segmental level and includes results from all three weight lifting tasks. 7b presents the main effect of load magnitude and includes results from all the four intervertebral segments. Magnitudes are normalized to the height of the respective inferior vertebral bodies of each segment (L5S1 data are normalized to height of L5). 100% represents the whole height of the vertebral body. COR represents, as a single value, the average of the all the ICRs across the participants.

4. Discussion

In order to better place current findings regarding ICR patterns in context with past studies, results are discussed further within the frame of three aspects of lumbar segmental translation: 1) amplitude of the centrode; (2) average COR location in the sagittal plane; and (3) direction of ICR migration vis-à-vis the corresponding rotational direction.

4.1. Amplitude of centrode

Average segmental centrodes recorded in the current study ranged between 85–150% of vertebral body depth over a segmental rotational ROM between 9–15°. These values are generally closer to the lower end of the range for L4L5 and L5S1 reported by past experimental studies. For example, (Ogston et al., 1986) reported 43 mm (range: 15–83 mm) and 56 mm (range 20–93.5 mm) for L4L5 and L5S1 joints respectively over a range 18° and 19° respectively from full extension to full flexion based on sequentially static lateral radiographs, or approximately 126% (range: 44–245%) – 165% (range: ~60–275%), assuming vertebral depth ~34 mm (Zhou et al., 2000). (Gertzbein et al., 1984) reported an average centrode of 21 ($\pm$8.56) mm [~62($\pm$25) %] for healthy L4L5 segments over a rotational ROM of 15°. Modelling studies – finite element (Schmidt et al., 2008a) and rigid body modelling (Abouhossein et al., 2013) – have generally reported smaller centrode values. The current study provides new data for the cranial segments L2L3 and L3L4, which had not been fully addressed in past studies.

The most unique insights, however, are revealed when analyzing the AP- and SI- components of the ICR migration patterns. Specifically, contrasting the AP range of ICR migration clearly showed cranial segments – L2L3 and to a smaller extent L3L4 – exhibiting larger translations compared to the caudal L4L5 and L5S1 segments.

4.2. Location of average COR

Segment-specific differences were clearly detected for SI coordinates of the averaged COR: CORs for the L2L3 and L3L4 segments were significantly inferiorly located in comparison to the caudal segments L4L5 and L5S1. Similar to a larger AP centrode component, a more inferiorly located COR is also a manifestation of larger coupled translations associated with segmental rotations. Larger AP translation could imply a lower shear resistance in cranial segments compared to the caudal segments, however documented evidence in the published literature on lumbar joint shear behavior (Lu et al., 2005; Nachemson et al., 1979; Oxland, 2016; Skrzypiec et al., 2012) is sparse. We found one supporting study (Gardner-Morse and Stokes, 2004), which reported L4L5 AP shear- as well as the coupled flexion-extension rotational stiffnesses to be about 20% larger than the corresponding values for L2L3.

While the present study clearly demonstrated substantial ICR migration (Figs. 3 and 4, Table 2), no significant differences were detected across segments in the averaged AP COR location. This could be attributed to averaging over a substantially large amount of AP translation. CORs, on average, were located between the vertebral body mid-coronal plane up to about 10% posterior from the mid-coronal plane, thus slightly more anterior compared to what has been reported by past studies (Abouhossein et al., 2013; Gertzbein et al., 1984; Pearcy et al., 1984; Xia et al., 2010), barring a few exceptions (Cossette et al., 1971; White and Panjabi, 1978). A recently published study (Liu et al., 2016) reported averaged L4L5 and L5S1 CORs located at 82% and 103% of the intervertebral disc lengths from the anterior edge respectively. Similarities of experimental technique with the current study notwithstanding – lumbar kinematics were obtained by imaging subjects performing a lifting task within a dynamic biplane fluoroscopic system – CORs from Liu et al.'s study are substantially posteriorly located compared to the current study. Two key differences could, at least partially, explain this apparent divergence in results. First, while

Table 3
Segmental level-specific ICR coordinates in the sagittal plane, averaged to a single COR value. Values represent mean ($\pm CI_{95}$) coordinate locations in AP and SI directions normalized to the vertebral body depth and height respectively. Dissimilar superscripts indicate significant difference.

Lumbar segment	AP ($\pm$95% CI) (% vertebral body depth)				SI ($\pm$95% CI) (% vertebral body height)			
	10lb	20lb	30lb	All tasks	10lb	20lb	30lb	All tasks
L2-L3	−8 (10)	−4 (8)	−1 (9)	**−5 (8)**	27 (20)	23 (15)	30 (13)	**27 (9)**[a]
L3-L4	−2 (7)	−1 (6)	−1 (6)	**−1 (6)**	30 (11)	29 (17)	30 (13)	**30 (7)**[a]
L4-L5	−6 (9)	−3 (4)	−6 (7)	**−5 (7)**	44 (11)	47 (14)	45 (14)	**45 (7)**[b]
L5-S1	−9 (4)	−9 (6)	−12 (7)	**−10 (6)**	46 (17)	42 (18)	55 (20)	**47 (9)**[b]

participants in the current study started from a greater torso-flexed position (~75°) up to upright, Liu et al.'s study started from a moderate flexion position (~45°) but proceeded further into maximum extension. Second, the methods for computing the ICRs were dissimilar. Liu et al. defined the ICR as the cross point (*intersection*) of projection lines of the superior vertebra's AP axis at two different postures onto the sagittal plane of the inferior vertebra, which seems to be based on the *Reauleux* method. The current study employed the helical axis technique.

4.3. Direction of ICR migration

While some studies reported ICRs moving along the direction of angular motion (Ahmadi et al., 2009; Ellingson and Nuckley, 2015; Ogston et al., 1986; Schmidt et al., 2008b), others have reported ICRs moving opposite to the rotational direction (Abouhossein et al., 2013); still others have reported a looped pattern: an initial path along the direction of motion followed by a change in direction to return close to the initial location (Gertzbein et al., 1984; Ogston et al., 1986).

With some exceptions, such as at the beginning of motion, the current study found ICRs broadly migrated from anterior to posterior location with progression of the extension task along with the direction of rotation: trend analysis showed significant negative slopes ($p < 0.05$ for slope < 0) for AP ICR translation in all cases. A biomechanical explanation for this pattern could be an inherent mechanism to minimize reaction forces experienced within the intervertebral disc. For example, it is known that flexed positions result in greater torques applied on the spine compared to the upright position, which are mainly counter-balanced by forces generated within the back muscles and passive tissue structures. These active and passive soft tissue forces in turn dictate the total joint reaction forces within the spine. A more anteriorly located ICR (and, consequently, the center of reaction) in the flexed position could effectively result in larger muscle moment arms, thus affording a greater mechanical capacity to counter-balance the external torque with lower muscle forces compared to a posteriorly located ICR. A recent modelling study demonstrated reductions in muscle activity (from 17.5% to 1.5%) and axial joint reaction forces (~20% reduction) by optimizing the joint center (or reaction center) for an upright standing position (Zander et al., 2016). Although the study only simulated a static, upright pose, their conclusions lend broad credence to the underlying mechanism of minimizing muscle and joint forces by optimizing joint center location.

Finally, the magnitude of load lifted (within the range tested) had a negligible effect on the AP component of ICR migration as well as the location of the averaged COR. This seems contrary to the rationale presented above; e.g. increased loading caused by lifting a larger load should have caused an anterior shift of the CORs. Rather the results only indicate an increase in SI range of ICR migration and slight (but not significant) upward shift of the SI COR coordinate, particularly for L5S1 (Figs. 2, 6c and 7c). SI ICR movement seemed rather random. SI translation slopes in more than the half the cases were not statistically different from zero. Patterns were mixed in the remaining cases (either positive or negative slope). Our previous analysis of segmental rotational motion also failed to detect any significant effect of the load magnitude (Aiyangar et al., 2015). Some past studies, which evaluated the effect of external loads on vertebral motion and orientation, but found no significant effect (Anderson et al., 1986; Lee and Chen, 2000), have suggested that body weight exhibited a predominant effect compared to external loads on the external torques generated. This would imply that the weights used in the current study were not large enough to elicit significant changes in segmental kinematics. It is equally plausible that the small sample size affected the results similarly. While the purported upward shift of the COR was not statistically significant, lifting the largest load weight most certainly effected an increase in the SI component of the range of ICR migrations. It is plausible that the largest load caused more deformation to occur within the intervertebral disc in the SI direction, resulting in the observed ICR migration along the SI direction. If true, this would imply that effects of larger loads on the spine are not necessarily manifested in changes in rotational kinematics or ICR locations in the AP direction *per se*, but rather specifically in the deformation patterns of the intervertebral discs. While investigating this particular point further is the beyond the scope of the current study, future analyses of the collected kinematic datasets, coupled with rigid body modelling to estimate the magnitudes and patterns of forces generated within the disc could shed more light on this question.

Several limitations of the current study should be noted. First, the study was limited to young, healthy and relatively slim participants, thus capturing a small subset of the general population of interest. Second, the small sample size prevented further investigation of sex differences in ICR migration patterns and likely contributed to the inability to reveal differences in ICR patterns due the different loads handled. The small sample size also constrained our ability to fully quantify temporal aspects of ICR migration in lumbar motion segments using rigorous statistical methods, although some interesting new insights into ICR migration patterns were revealed. Third, as this was, first and foremost, a lifting task study, only extension motion was investigated. Hyperextension, forward flexion, lateral bending and twisting movements were not studied in consideration of a multitude of practical issues including the radiation exposure limit.

Conflicts of interest statement

The authors have no conflict of interest related to the manuscript or the work it describes.

Disclaimer

The findings and conclusions in this report are those of the authors and do not necessarily represent the views of the National Institute for Occupational Safety and Health.

Acknowledgments

The work was funded by a research grant (R21OH00996) from the Centers for Disease Control and Prevention/National Institute for Occupational Safety and Health (CDC/NIOSH). Additional support was received through the Marie Sklowdoska-Curie Cofund postdoctoral fellowship award (EMPAPOSTDOCS 267161) and Ambizione Career Grant Award (PZ00P2_154855/1) from the Swiss National Science Foundation (SNSF). The authors thank Dr. Scott Tashman for technical advice on DSX data acquisition. The authors also thank Robert Carey for assistance with conducting the tests and Jonathan Foster, Michelle Schafman, George Kontogiannis, and Eric Ruth for assistance with data processing. The authors acknowledge Matthew Bottegal's and Chelsea Marsh's assistance in recruiting participants for the study.

References

Abouhossein, A., Weisse, B., Ferguson, S.J., 2013. Quantifying the centre of rotation pattern in a multi-body model of the lumbar spine. Comput. Methods Biomech. Biomed. Eng. 16, 1362–1373.

Ahmadi, A., Maroufi, N., Behtash, H., Zekavat, H., Parnianpour, M., 2009. Kinematic analysis of dynamic lumbar motion in patients with lumbar segmental instability using digital videofluoroscopy. Eur. Spine J. 18, 1677–1685.

Aiyangar, A., Zheng, L., Anderst, W., Zhang, X., 2015. Apportionment of lumbar L2-S1 rotation across individual motion segments during a dynamic lifting task. J. Biomech. 48, 3718–3724.

Aiyangar, A.K., Zheng, L.Y., Tashman, S., Anderst, W.J., Zhang, X.D., 2014. Capturing three-dimensional in vivo lumbar intervertebral joint kinematics using dynamic stereo-x-ray imaging. J. Biomech. Eng. T ASME 136, 011004.

Anderson, C.K., Chaffin, D.B., Herrin, G.D., 1986. A study of lumbosacral orientation under varied static loads. Spine 11, 456–462.

Anderst, W., Baillargeon, E., Donaldson, W., Lee, J., Kang, J., 2013. Motion path of the instant center of rotation in the cervical spine during in vivo dynamic flexion-extension: implications for artificial disc design and evaluation of motion quality following arthrodesis. Spine.

Anderst, W.J., Vaidya, R., Tashman, S., 2008. A technique to measure three-dimensional in vivo rotation of fused and adjacent lumbar vertebrae. Spine J.: Off. J. N. Am. Spine Soc. 8, 991–997.

Baillargeon, E., Anderst, W.J., 2013. Sensitivity, reliability and accuracy of the instant center of rotation calculation in the cervical spine during in vivo dynamic flexion-extension. J. Biomech. 46, 670–676.

Bogduk, N., Amevo, B., Pearcy, M., 1995. A biological basis for instantaneous centres of rotation of the vertebral column. Proc. Inst. Mech. Eng. Part H J. Eng. Med. 209, 177–183.

Cossette, J.W., Farfan, H.F., Robertson, G.H., Wells, R.V., 1971. The instantaneous center of rotation of the third lumbar intervertebral joint. J. Biomech. 4, 149–153.

Crisco 3rd, J.J., Chen, X., Panjabi, M.M., Wolfe, S.W., 1994. Optimal marker placement for calculating the instantaneous center of rotation. J. Biomech. 27, 1183–1187.

Ellingson, A.M., Nuckley, D.J., 2015. Altered helical axis patterns of the lumbar spine indicate increased instability with disc degeneration. J. Biomech. 48, 361–369.

Freudiger, S., Dubois, G., Lorrain, M., 1999. Dynamic neutralisation of the lumbar spine confirmed on a new lumbar spine simulator in vitro. Arch. Orthop. Trauma Surg. 119, 127–132.

Fujii, R., Sakaura, H., Mukai, Y., Hosono, N., Ishii, T., Iwasaki, M., Yoshikawa, H., Sugamoto, K., 2007. Kinematics of the lumbar spine in trunk rotation: in vivo three-dimensional analysis using magnetic resonance imaging. Eur. Spine J. 16, 1867–1874.

Gardner-Morse, M.G., Stokes, I.A., 2004. Structural behavior of human lumbar spinal motion segments. J. Biomech. 37, 205–212.

Gertzbein, S.D., Holtby, R., Tile, M., Kapasouri, A., Chan, K.W., Cruickshank, B., 1984. Determination of a locus of instantaneous centers of rotation of the lumbar disc by moire fringes. A new technique. Spine 9, 409–413.

Gertzbein, S.D., Seligman, J., Holtby, R., Chan, K.H., Kapasouri, A., Tile, M., Cruickshank, B., 1985. Centrode patterns and segmental instability in degenerative disc disease. Spine 10, 257–261.

Gertzbein, S.D., Seligman, J., Holtby, R., Chan, K.W., Ogston, N., Kapasouri, A., Tile, M., 1986. Centrode characteristics of the lumbar spine as a function of segmental instability. Clin. Orthop. Relat. Res., 48–51.

Han, K.S., Kim, K., Park, W.M., Lim, D.S., Kim, Y.H., 2013. Effect of centers of rotation on spinal loads and muscle forces in total disk replacement of lumbar spine. Proc. Inst. Mech. Eng. Part H J. Eng. Med. 227, 543–550.

Kozanek, M., Wang, S., Passias, P.G., Xia, Q., Li, G., Bono, C.M., Wood, K.B., Li, G., 2009. Range of motion and orientation of the lumbar facet joints in vivo. Spine 34, E689–696.

Lee, J.B.E.; Anderst, W.J., 2010. Lumbar spine motion during functional movement: in vivo validation of flexion/extension movement tracking. In: Proceedings of the 3rd Annual Lumbar Spine ResearchSociety Meeting, Chicago, IL, USA.

Lee, Y.H., Chen, Y.L., 2000. Regressionally determined vertebral inclination angles of the lumbar spine in static lifts. Clin. Biomech. 15, 672–677.

Li, W.S., Wang, S.B., Xia, Q., Passias, P., Kozanek, M., Wood, K., Li, G.A., 2011. Lumbar facet joint motion in patients with degenerative disc disease at affected and adjacent levels an in vivo biomechanical study. Spine 36, E629–E637.

Liu, Z., Tsai, T.Y., Wang, S., Wu, M., Zhong, W., Li, J.S., Cha, T., Wood, K., Li, G., 2016. Sagittal plane rotation center of lower lumbar spine during a dynamic weight-lifting activity. J. Biomech. 49, 371–375.

Lu, W.W., Luk, K.D., Holmes, A.D., Cheung, K.M., Leong, J.C., 2005. Pure shear properties of lumbar spinal joints and the effect of tissue sectioning on load sharing. Spine 30, E204–209.

Martin, D.E., Greco, N.J., Klatt, B.A., Wright, V.J., Anderst, W.J., Tashman, S., 2011. Model-based tracking of the hip: implications for novel analyses of hip pathology. J. Arthroplast. 26, 88–97.

Mcgill, R., Tukey, J.W., Larsen, W.A., 1978. Variations of box plots. Am. Stat. 32, 12–16.

Nachemson, A.L., Schultz, A.B., Berkson, M.H., 1979. Mechanical properties of human lumbar spine motion segments. Influence of age, sex, disc level, and degeneration. Spine 4, 1–8.

Natarajan, R.N., Williams, J.R., Lavender, S.A., An, H.S., Anderson, G.B., 2008. Relationship between disc injury and manual lifting: a poroelastic finite element model study. Proc. Inst. Mech. Eng. Part H J. Eng. Med. 222, 195–207.

Ochia, R.S., Inoue, N., Renner, S.M., Lorenz, E.P., Lim, T.H., Andersson, G.B., An, H.S., 2006. Three-dimensional in vivo measurement of lumbar spine segmental motion. Spine 31, 2073–2078.

Ogston, N.G., King, G.J., Gertzbein, S.D., Tile, M., Kapasouri, A., Rubenstein, J.D., 1986. Centrode patterns in the lumbar spine. Baseline studies in normal subjects. Spine 11, 591–595.

Oxland, T.R., 2016. Fundamental biomechanics of the spine–What we have learned in the past 25 years and future directions. J. Biomech. 49, 817–832.

Passias, P.G., Wang, S.B., Kozanek, M., Xia, Q., Li, W.S., Grottkau, B., Wood, K.B., Li, G. A., 2011. Segmental lumbar rotation in patients with discogenic low back pain during functional weight-bearing activities. J. Bone Jt. Surg. Am. 93A, 29–37.

Pearcy, M., Portek, I., Shepherd, J., 1984. Three-dimensional x-ray analysis of normal movement in the lumbar spine. Spine 9, 294–297.

R_Core_Team, 2015. R: A Language and Environment for Statistical Computing. R Foundation for Statistical Computing, Vienna, Austria.

Schmidt, H., Heuer, F., Wilke, H.J., 2008b. Interaction between finite helical axes and facet joint forces under combined loading. Spine 33, 2741–2748.

Schmidt, H., Heuer, F., Claes, L., Wilke, H.J., 2008a. The relation between the instantaneous center of rotation and facet joint forces - a finite element analysis. Clin. Biomech. 23, 270–278.

Schneider, G., Pearcy, M.J., Bogduk, N., 2005. Abnormal motion in spondylolytic spondylolisthesis. Spine 30, 1159–1164.

Skrzypiec, D.M., Klein, A., Bishop, N.E., Stahmer, F., Puschel, K., Seidel, H., Morlock, M.M., Huber, G., 2012. Shear strength of the human lumbar spine. Clin. Biomech. 27, 646–651.

Spoor, C.W., Veldpaus, F.E., 1980. Rigid body motion calculated from spatial coordinates of markers. J. Biomech. 13, 391–393.

Teyhen, D.S., Flynn, T.W., Childs, J.D., Kuklo, T.R., Rosner, M.K., Polly, D.W., Abraham, L.D., 2007. Fluoroscopic video to identify aberrant lumbar motion. Spine 32, E220–229.

White 3rd, A.A., Panjabi, M.M., 1978. The basic kinematics of the human spine. A review of past and current knowledge. Spine 3, 12–20.

Wong, K.W., Leong, J.C., Chan, M.K., Luk, K.D., Lu, W.W., 2004. The flexion-extension profile of lumbar spine in 100 healthy volunteers. Spine 29, 1636–1641.

Wu, G., Siegler, S., Allard, P., Kirtley, C., Leardini, A., Rosenbaum, D., Whittle, M., D'Lima, D.D., Cristofolini, L., Witte, H., Schmid, O., Stokes, I., Standardization, Terminology Committee of the International Society of, B., 2002. ISB recommendation on definitions of joint coordinate system of various joints for the

reporting of human joint motion – Part I: ankle, hip, and spine. Int. Soc. Biomech. J. Biomech. 35, 543–548.
Wu, M., Wang, S., Driscoll, S.J., Cha, T.D., Wood, K.B., Li, G., 2014. Dynamic motion characteristics of the lower lumbar spine: implication to lumbar pathology and surgical treatment. Eur. Spine J. 23, 2350–2358.
Xia, Q., Wang, S.B., Kozanek, M., Passias, P., Wood, K., Li, G.A., 2010. In-vivo motion characteristics of lumbar vertebrae in sagittal and transverse planes. J. Biomech. 43, 1905–1909.
Zander, T., Rohlmann, A., Bergmann, G., 2009. Influence of different artificial disc kinematics on spine biomechanics. Clin. Biomech. 24, 135–142.
Zander, T., Dreischarf, M., Schmidt, H., 2016. Sensitivity analysis of the position of the intervertebral centres of reaction in upright standing – a musculoskeletal model investigation of the lumbar spine. Med. Eng. Phys. 38, 297–301.
Zhou, S.H., McCarthy, I.D., McGregor, A.H., Coombs, R.R., Hughes, S.P., 2000. Geometrical dimensions of the lower lumbar vertebrae–analysis of data from digitised CT images. Eur. Spine J. 9, 242–248.
Zhu, R., Zander, T., Dreischarf, M., Duda, G.N., Rohlmann, A., Schmidt, H., 2013. Considerations when loading spinal finite element models with predicted muscle forces from inverse static analyses. J. Biomech. 46, 1376–1378.